Van der Waals epitaxy of ultrathin α-MoO3 sheets on mica substrate with single-unit-cell thickness

Di Wang, Jing-Ning Li, Yu Zhou, Di-Hu Xu, Xiang Xiong, Ru-Wen Peng, and Mu Wang

Citation: Applied Physics Letters **108**, 053107 (2016); doi: 10.1063/1.4941402
View online: http://dx.doi.org/10.1063/1.4941402
View Table of Contents: http://scitation.aip.org/content/aip/journal/apl/108/5?ver=pdfcov
Published by the AIP Publishing

Van der Waals epitaxy of ultrathin α-MoO_3 sheets on mica substrate with single-unit-cell thickness

Di Wang, Jing-Ning Li, Yu Zhou, Di-Hu Xu, Xiang Xiong, Ru-Wen Peng, and Mu Wang[a)]
National Laboratory of Solid State Microstructures and Department of Physics and Collaborative Innovation Center of Advanced Microstructures, Nanjing University, Nanjing 210093, China

(Received 16 July 2015; accepted 25 January 2016; published online 5 February 2016)

We report on van der Waals epitaxy of single-crystalline α-MoO_3 sheets with single-unit-cell thickness on the mica substrate. The crystalline lattice structure, growth habits, and Raman spectra of the grown α-MoO_3 sheets are analyzed. The anisotropic growth of α-MoO_3 sheets can be understood by period bond chains theory. Unlike monolayer MoS_2 or graphene, Raman spectra of α-MoO_3 do not possess frequency shift from bulk crystal to single-unit-cell layer. The relative intensities of two Raman modes (A_g) at 159 and 818 cm^{-1} are sensitive to the polarization of incident light. This scenario provides a quick approach to determine the lattice orientation of α-MoO_3 crystals. Our studies indicate that van der Waals epitaxial growth is a simple and effective way to fabricate high-quality ultrathin α-MoO_3 sheets for physical property investigations and potential applications. © *2016 AIP Publishing LLC*. [http://dx.doi.org/10.1063/1.4941402]

When the thickness of molybdenum disulfide (MoS_2) layer approaches the atomic-scale, various intriguing properties emerge, which are distinct from that of the bulk MoS_2. Unlike its bulk counterpart, monolayer MoS_2 is a direct-bandgap semiconductor with a bandgap of ~1.89 eV, which can be applied to fabricate field effect transistors (FET) with high efficiency[1] and to enhance the photoluminescence effectively in the visible frequency range.[2] Monolayer MoS_2 without inversion symmetry exhibits a strong spin-orbit coupling, which combines electron spin and K-valley in the Brillouin zone. Therefore, it is possible to manipulate K-valley index of electrons with circularly polarized light.[3]

The molybdenum trioxide (α-MoO_3) is another molybdenum compound with layered structure. The interests in α-MoO_3 originate from its high κ-dielectric (>200),[4] high work function (~6.8 eV),[5] good transparency to visible light, and the controllable semiconducting properties.[6] The high-κ value is beneficial in reducing Coulomb scattering effectively, and the charge carrier mobility of a α-MoO_3 FET device can reach 1100 $cm^2 V^{-1} s^{-1}$.[7] In light emitting diodes (LED), solar cell and photovoltaic (PV), α-MoO_3 is an efficient hole-transport interlayer between the anode and the active layer.[8] The composite of α-MoO_3 and carbon nanotube (CNT) is promising to serve as the practical transparent electrodes.[9] In addition, the intrinsic layered structure of α-MoO_3 provides flexibilities for energy-band engineering via H^+ and Li^+ ion intercalation.[10]

The α-MoO_3 crystal is composed of planar slabs of double-layered [MoO_6] octahedra, which are stacked vertically in ⟨010⟩ via weak van der Waals forces. Within the planar slab, [MoO_6] octahedra are bound by covalent bonds.[11] It is possible to obtain 2D structure of α-MoO_3 with a thickness of atomic level. Comparing to its bulk counterpart, a-few-layered α-MoO_3 sheet exhibits superior properties in catalytic, optical, and energy-storage application.[12–14] However, up until now, it remains challenging to obtain large and uniform α-MoO_3 sheets with thickness of a few unit cells. Van der Waals epitaxy has been considered as an ideal approach to fabricate 2D materials.[15] Since there is no dangling bond connecting the epitaxial layer and the substrate, the lattice matching condition can be relaxed and the growth temperature can be decreased.[16,17]

Here, we report on van der Waals epitaxial growth of ultrathin α-MoO_3 sheets on fluorophlogopite mica ($KMg_3AlSi_3O_{10}F_2$) via an ambient pressure physical vapor deposition (APPVD). The grown single-crystalline α-MoO_3 sheets are highly *b*-axis oriented on mica, and the lateral size reaches several tens of micrometers. The thickness of the α-MoO_3 sheet can be controlled from 1.4 nm to several micrometers by controlling the growth temperature. Raman spectra of α-MoO_3 sheets indicate that the relative intensities of the Raman modes (A_g) are sensitive to the polarization of incident light. The growth habits of α-MoO_3 sheets on the mica substrate are also discussed.

The α-MoO_3 sheets are grown in a homemade dual-temperature zone furnace. The MoO_3 powder is vaporized in the high-temperature zone and ultrapure N_2 gas (99.999%) serves as the carry gas with ambient pressure. The vaporization temperature is gradually increased to 600 °C from room temperature in 60 min. The freshly cleaved fluorophlogopite mica is located in the growth zone, and the growth temperature is set between 350 °C and 480 °C. The distance between the MoO_3 source and the mica is 40 cm. The typical growth time is 20 min, after the growth the furnace is cooled down to room temperature naturally.

The phase information of α-MoO_3 sheets is analyzed with grazing incidence X-ray diffraction (GIXRD, Rigaku MAX-RD). Surface morphology is characterized by a Nikon optical microscope (ECLIPSE 80i). The thickness of the α-MoO_3 sheet is measured by an atom force microscopy (AFM; Digital Instruments Multimode™ SPM). The crystallographic structure of the α-MoO_3 sheet is determined by a high resolution transmission electron microscope (HRTEM; JEOL JEM-1011). Raman spectra are collected using a

a)Email: muwang@nju.edu.cn

confocal micro-Raman system (Princeton Instrument). The laser wavelength is 514.5 nm, and the spot size is about 2 μm. The incident light polarization is fixed, while the sample is rotated in order to change the angle θ between the incident light polarization and c axis of the crystalline sheet of α-MoO_3. No analyzer is applied in the Raman spectrometer.

Theoretical Raman frequencies, intensities, and scattering tensors of the α-MoO_3 crystal have been calculated with density functional perturbation theory (DFPT).[18] Calculations are performed using Generalized Gradient Approximation with norm-conserving pseudopotential. The kinetic energy cutoff for the plane-wave basis set is 830 eV. $(9 \times 2 \times 9)$ K-point sampling is used for Brillouin zone integration. The convergence criterion of self-consistent calculations for ionic relaxations is set as 10^{-5} eV.

Figure 1(a) shows a typical optical micrograph of α-MoO_3 sheets grown on mica substrate. The rectangular flakes are the grown α-MoO_3 sheets, and the darker background is the mica substrate. The rectangular α-MoO_3 sheets mostly align in three major orientations 120° with each other, which signify the nature of van der Waals epitaxial growth.[16,17]

The growth temperature is important to control the size and the thickness of the α-MoO_3 sheet. At high growth temperature, high saturation vapor pressure of MoO_3, and small nucleation rate is expected. Moreover, the growth units have a high probability of diffusing to their edge sites at high temperature, and the crystal prefers the planar growth on substrate.[19] These would result in large and ultrathin α-MoO_3 sheet growth. We grow α-MoO_3 sheets at several different temperatures, and find the sheet thickness indeed depends on the growth temperature (Fig. 1(b)). When the growth temperature is increased, the thickness of α-MoO_3 sheets decreases, and the sheet size increases.

The phase of the grown α-MoO_3 sheets is determined by GIXRD. In order to obtain high signal-to-noise ratio, we measure the diffraction signals from thick MoO_3 sheets (>50 nm), as illustrated in Fig. 1(c). The diffraction peaks can be indexed as (0,2,0), (0,4,0), (0,6,0), and (0,10,0) of the orthorhombic structured MoO_3 crystal (International Centre for Diffraction Data, No05–0508, lattice constants of $a = 3.962$ Å, $b = 13.858$ Å, and $c = 3.697$ Å). The fact that only diffraction of (0, l, 0) is observable suggests that the grown α-MoO_3 sheets are highly b-axis-oriented. The lattice structures are further investigated by HRTEM as illustrated in Fig. 1(d). The HRTEM micrograph shows that the lattice distances of $d_{(0,0,1)} = 0.36$ nm and $d_{(1,0,0)} = 0.39$ nm, which are in agreement with the parameters of (0,l,0) for α-MoO_3 crystal.[20] The selected-area electron diffraction (SAED) pattern (inset of Fig. 1(d)) reveals that the longitudinal direction of the grown MoO_3 sheets is parallel with $\langle 001 \rangle$.

The planar slab of α-MoO_3 crystal consists of bilayer (BL) of [MoO_6] octahedra. The unit cell spans two BLs along b-axis (Fig. 2(a)). Figure 2(b) illustrates AFM micrograph of an ultrathin α-MoO_3 sheet, which possesses a lateral size above 30 μm and a thickness of single-unit cell (~1.4 nm). In present work, α-MoO_3 sheets with various thicknesses (from 2 to 10 BLs) are grown on mica, and their topographic micrographs and line profiles are obtained by AFM, as shown in Figs. 2(b)–2(f), respectively.

The Raman spectra of α-MoO_3 sheets are experimentally measured and theoretically calculated, as shown in Fig. 3. It can be seen that the calculated spectrum is similar

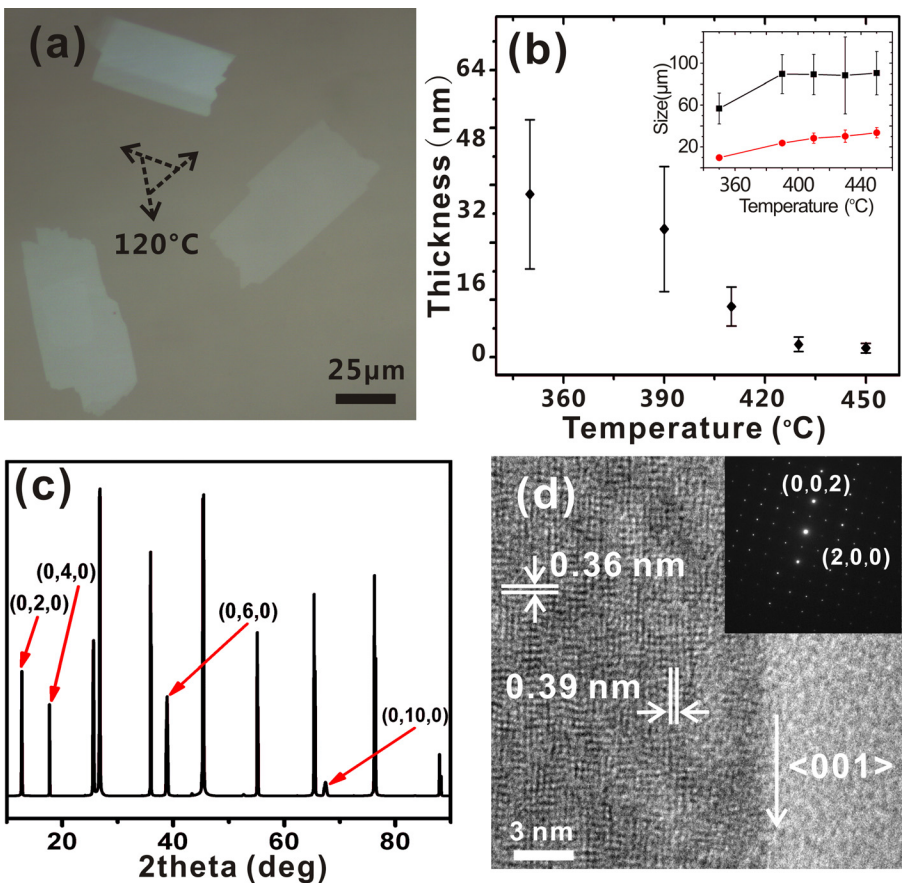

FIG. 1. (a) Optical micrograph of grown α-MoO_3 sheets on mica substrate. The dashed arrows denote three growth orientations. (b) Thicknesses and sizes (inset) of α-MoO_3 sheets as a function of the growth temperature. The statistics is obtained from twenty samples with the area of ~4 × 5 mm. (c) The GIXRD pattern of grown α-MoO_3 sheets on the mica substrate. Diffraction peaks of the α-MoO_3 sheet are marked by red arrows. (d) The HRTEM image and the SAED pattern (inset) of the α-MoO_3 sheet.

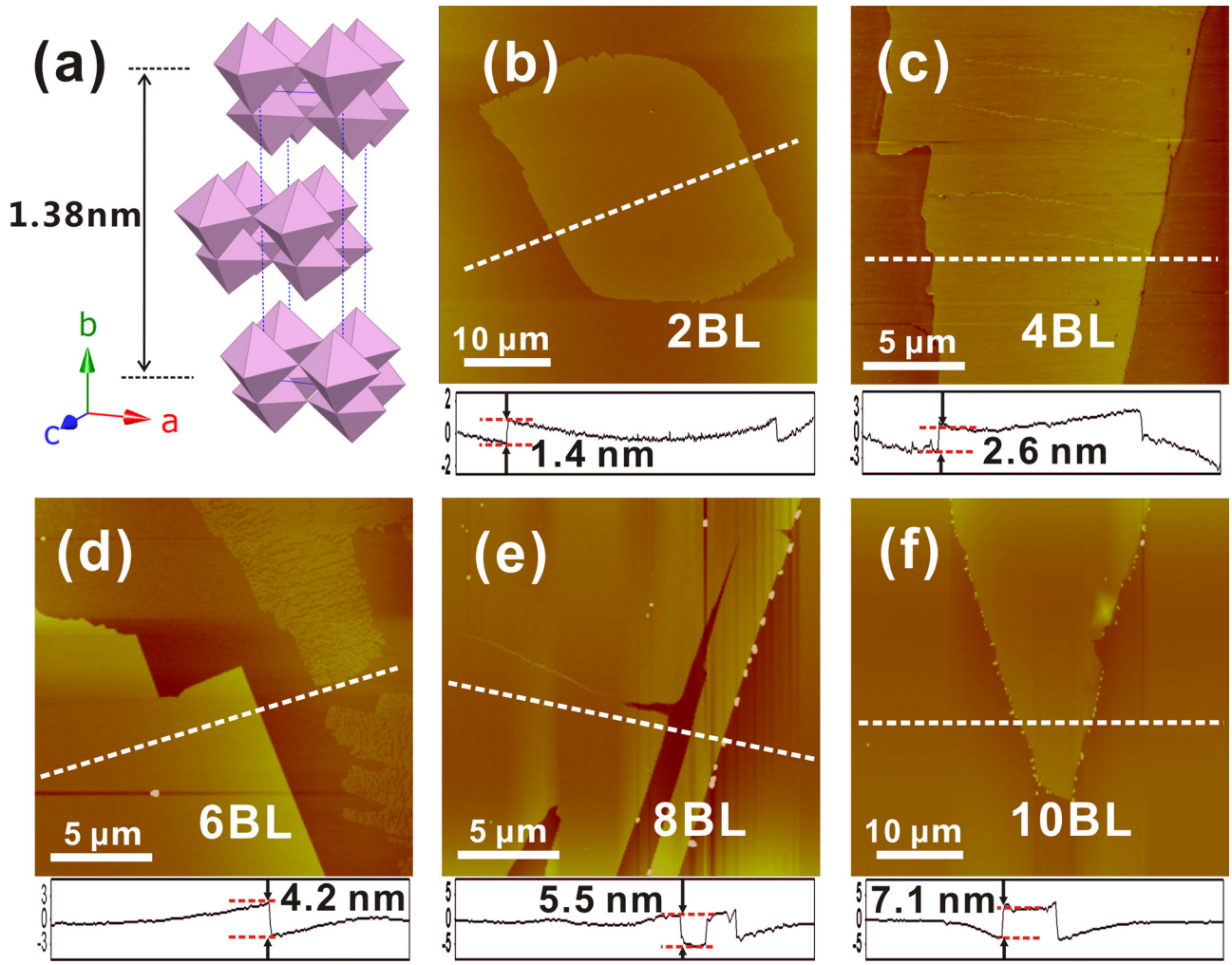

FIG. 2. (a) Crystalline structure of the α-MoO_3 crystal. (b)–(f) AFM micrographs and height profiles of α-MoO_3 sheets with various thicknesses. The height profile is taken along the dashed line in the corresponding AFM image.

to that of the experimental measurement. The strongest peak locates around 820 cm^{-1} in experiment, corresponding to that at 802 cm^{-1} in theory. Both space group analysis[21] and DFPT calculation suggest that the Raman peaks of α-MoO_3 are attributed by the vibration modes of Mo-O bonds.[22] In the planar slab, [MoO_6] octahedra interconnect by edge-sharing zig-zag rows along the ⟨001⟩, and interconnect by corner-sharing rows along ⟨100⟩ (Fig. 2(a)). Six oxygen atoms in each [MoO_6] octahedron can be categorized into three types: one terminal-oxygen atom (denoted as O_1) belonging to individual octahedron, two corner-shared oxygen atoms (denoted as O_2) shared by two adjacent octahedra, and three edge-shared oxygen atoms (denoted as O_3) shared by three adjacent octahedral. Raman peak at 998 cm^{-1} is associated with the stretching vibration of Mo-O_1 bonds along *b* axis (A_g mode), corresponding to that at 993 cm^{-1} in theory; the 820 cm^{-1} peak is associated with the stretching vibration of the Mo-O_2-Mo bond along *a* axis (A_g mode); the 159 cm^{-1} peak originates from the translation vibration of the rigid chains along *c* axis (A_g mode), corresponding to that at 142 cm^{-1} in theory. Because the grown α-MoO_3 sheets parallel to (0,*l*,0) faces, the in-plane vibration peak of 820 cm^{-1} is strong; in contrast, the out-of-plane vibration peak of 998 cm^{-1} is very weak.

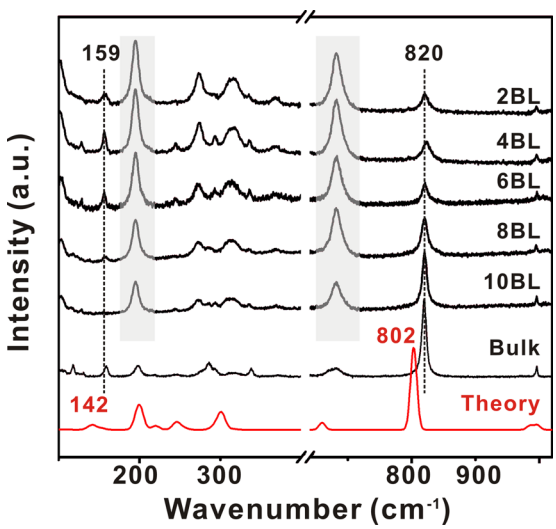

FIG. 3. The calculated Raman spectrum of the bulk α-MoO_3 crystal (red) and experimental Raman spectra of the α-MoO_3 sheets with various thicknesses. The peaks in the gray zone are attributed to Raman peaks of the mica substrate.

It should be noted that DFPT calculation usually underestimates the Raman frequencies. The deviations of A_g modes at 998, 882, and 159 cm^{-1} reach 0.5%, 2%, and 10%, respectively. These deviations may originate from the

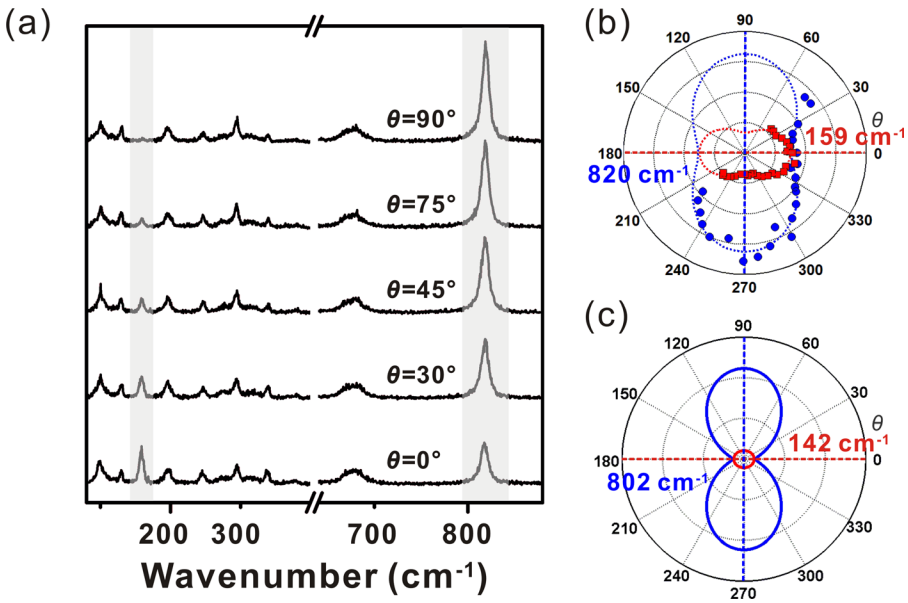

FIG. 4. (a) Raman spectra of α-MoO_3 sheets as the function of polarization angle θ. θ denotes the angle between the incident light polarization and c axis of an α-MoO_3 crystal. (b) The angle-dependent intensities of 820 and 159 cm^{-1} peaks measured from the experimental spectra, the blue and red dashed lines are the fitting curves. (c) The angle-dependent intensities calculated using Raman scattering tensor R in DFPT theory.

density-functional theory (DFT) calculation, the first step calculation of DFPT to obtain unperturbed periodic ground state, which usually underestimates energy band gap and lattice constant.[23] Especially, the low frequency peak at 159 cm^{-1} (the softer mode) is more sensitive to ground state energy and lattice structure,[24] hence has a large deviation of Raman frequency.

The Raman spectra of α-MoO_3 sheets with different thickness are also shown in Fig. 3. The positions of Raman peaks do not change when the sheet thickness decreases, yet the peak intensity decreases with respect to that of the mica substrate. This scenario is different from thickness-dependent Raman spectra of MoS_2.[25] The unique features of the Raman frequencies of α-MoO_3 may result from the weak interlayer coupling among the double-[MoO_6] layers. The bulk α-MoO_3 crystal behaves just like the decoupled stack of planer layers.

It is noteworthy that the relative intensities of two A_g Raman peaks at 159 and 820 cm^{-1} exhibit a clear dependence on the incident light polarization (Figs. 4(a) and 4(b)). A similar phenomenon has been reported for $ReSe_2$,[26] which elucidated the angle-dependent intensity by the Raman scattering tensors R of vibration mode. In our case, Raman vibration modes and scattering tensors R of 159 and 820 cm^{-1} have been obtained from DFPT calculation. The angle-dependent intensities are calculated and shown in Fig. 4(c), which is in consistent with experimental results. When the incidence polarization parallels to a axis, Raman peak at 820 cm^{-1} reaches its strongest intensity, and that at 159 cm^{-1} reaches its weakest intensity. In contrast, when the incidence polarization parallels to c axis, the peak at 820 cm^{-1} reaches its weakest intensity, and that at 159 cm^{-1} reaches its strongest intensity. Due to this strong correlation between the lattice orientation and Raman scattering intensity, we are able to determine quickly the a and c axes based on the relative intensity of Raman peaks at 820 and 159 cm^{-1}.

The growth habits of α-MoO_3 sheets on the mica substrate, such as the well-defined lattice orientation and the anisotropic growth, can be understood by period bond chain (PBC) theory.[27] The PBC theory suggests that the growth rate of crystallographic faces is determined by a set of uninterrupted bond chains formed in crystallization. For α-MoO_3 crystal, the bond chains involve covalent bond chains within the planar layers and van der Waals bond chains between the layers. Comparing to the weak van der Waals bonds, in-plate Mo-O covalent bonds are much stronger. Therefore, α-MoO_3 crystal prefers two-dimensional lateral growth of (0,l,0) planes.

On the other hand, Mo-O covalent bond chains in (0,l,0) can be classified into two types: Mo-O_3-Mo bond chains are along ⟨001⟩, where [MoO_6] octahedra are interconnected with their edges; and Mo-O_2-Mo bond chains are along ⟨100⟩, where [MoO_6] octahedra are interconnected with their corners. The former has a stronger bond energy than the later. Therefore, (0,0,1) faces grow faster than (1,0,0) faces. Figure 5(a) shows an AFM micrograph of a typical α-MoO_3 sheet grown on mica. Remarkable features of layer-by-layer growth can be observed. The growth front of each layer is rough, but the edges perpendicular to the growth direction are straight and sharp (Figs. 5(b) and 5(c)). The crystallographic structural analysis based on TEM data (Fig. 1(d)) indicates that the long edge parallels with ⟨001⟩, where Mo-O_3-Mo bond chains lie, and the rough growing interface parallels with the ⟨100⟩, along which Mo-O_2-Mo bond

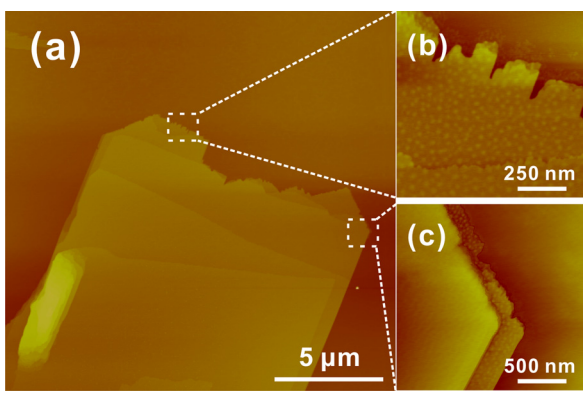

FIG. 5. (a) A typical AFM image of an α-MoO_3 sheet. (b) and (c) The enlarged micrographs of the dashed boxed regions in (a).

chains lie. We can conclude that for van der Waals epitaxial growth of ultrathin α-MoO_3 sheets, the period Mo-O bond chains in the planar layer determine the anisotropic growth habit.

To summarize, we have grown large and uniform α-MoO_3 sheets with single-unit-cell thickness via van der Waals epitaxy on mica. It is shown that the growth temperature is critical in controlling the sheet thickness. Experiments show that Raman peaks of α-MoO_3 sheets do not shift when the sheet thickness varies, yet the peak intensities of A_g vibration modes are sensitive to the incidence polarization. This study shows that van der Waals epitaxy is a simple and effective approach for fabricating of ultrathin α-MoO_3 sheets.

This work has been supported by the grants from the National Natural Science Foundation of China (NSFC) (Grant Nos. 51302268, 11474157, 11034005, 11574141, and 61475070), the Ministry of Science and Technology of China (MOST) (Grant Nos. 2010CB630705 and 2012CB921502), and the Ministry of Education of the People's Republic of China (MOE) (SRFDP No. 20120091120033).

[1]B. Radisavljevic, A. Radenovic, J. Brivio, V. Giacometti, and A. Kis, Nat. Nano **6**(3), 147 (2011).
[2]A. Splendiani, L. Sun, Y. B. Zhang, T. S. Li, J. Kim, C. Chim, G. Galli, and F. Wang, Nano Lett. **10**(4), 1271 (2010).
[3]H. L. Zeng, J. F. Dai, W. Yao, D. Xiao, and X. D. Cui, Nat. Nano **7**(8), 490 (2012).
[4]S. Balendhran, S. Walia, H. Nili, J. Z. Ou, S. Zhuiykov, R. B. Kaner, S. Sriram, M. Bhaskaran, and K. Kalantar-zadeh, Adv. Funct. Mater. **23**(32), 3952 (2013).
[5]J. Meyer, S. Hamwi, M. Kröger, W. Kowalsky, T. Riedl, and A. Kahn, Adv. Mater. **24**(40), 5408 (2012).
[6]S. Y. Lin, C. M. Wang, K. S. Kao, Y. C. Chen, and C. C. Liu, J. Sol-Gel Sci. Technol. **53**(1), 51 (2010).
[7]S. Balendhran, J. K. Deng, J. Z. Ou, S. Walia, J. Scott, J. S. Tang, K. L. Wang, M. R. Field, S. Russo, S. Zhuiykov, M. S. Strano, N. Medhekar, S. Sriram, M. Bhaskaran, and K. Kalantar-zadeh, Adv. Mater. **25**(1), 109 (2013).
[8]P. Schulz, S. R. Cowan, Z. L. Guan, A. Garcia, D. C. Olson, and A. Kahn, Adv. Funct. Mater. **24**(5), 701 (2014).
[9]S. L. Hellstrom, M. Vosgueritchian, R. M. Stoltenberg, I. Irfan, M. Hammock, Y. B. Wang, C. C. Jia, X. F. Guo, Y. L. Gao, and Z. N. Bao, Nano Lett. **12**(7), 3574 (2012).
[10]Y. A. Yang, Y. W. Cao, B. H. Loo, and J. N. Yao, J. Phys. Chem. B **102**(47), 9392 (1998).
[11]S. Guimond, D. Göbke, J. M. Sturm, Y. Romanyshyn, H. Kuhlenbeck, M. Cavalleri, and H.-J. Freund, J. Phys. Chem. C **117**(17), 8746 (2013).
[12]I. Hancox, K. V. Chauhan, P. Sullivan, R. A. Hatton, A. Moshar, C. P. A. Mulcahy, and T. S. Jones, Energy Environ. Sci. **3**(1), 107 (2010).
[13]Y. X. Wang, X. Zhang, Z. M. Luo, X. Huang, C. L. Tan, H. Li, B. Zheng, B. Li, Y. Huang, J. Yang, Y. Zong, Y. B. Ying, and H. Zhang, Nanoscale **6**(21), 12340 (2014).
[14]M. M. Y. A. Alsaif, K. Latham, M. R. Field, D. D. Yao, N. V. Medehkar, G. A. Beane, R. B. Kaner, S. P. Russo, J. Z. Ou, and K. Kalantar-zadeh, Adv. Mater. **26**(23), 3931 (2014).
[15]A. Koma, J. Cryst. Growth **201–202**(0), 236 (1999).
[16]Q. Q. Ji, Y. F. Zhang, T. Gao, Y. Zhang, D. L. Ma, M. X. Liu, Y. B. Chen, X. F. Qiao, P. H. Tan, M. Kan, J. Feng, Q. Sun, and Z. F. Liu, Nano Lett. **13**(8), 3870 (2013).
[17]W. H. Dang, H. L. Peng, H. Li, P. Wang, and Z. F. Liu, Nano Lett. **10**(8), 2870 (2010).
[18]S. Baroni, S. de Gironcoli, A. Dal Corso, and P. Giannozzi, Rev. Mod. Phys. **73**(2), 515 (2001).
[19]I. V. Markov, *Crystal Growth for Beginners* (World Scientific, Singapore, 2003), p. 492.
[20]L. Kihlborg, Arkiv for Kemi **21**(34), 357 (1963).
[21]B. C. Windom, W. G. Sawyer, and D. W. Hahn, Tribol. Lett. **42**(3), 301 (2011).
[22]M. A. Py, Ph. E. Schmid, and J. T. Vallin, Nuov Cimento B **38**(2), 271 (1977).
[23]L. Lajaunie, F. Boucher, R. Dessapt, and P. Moreau, Phys. Rev. B **88**(11), 115141 (2013).
[24]Z. G. Wu, R. E. Cohen, and D. J. Singh, Phys. Rev. B **70**(10), 104112 (2004).
[25]C. G. Lee, H. G. Yan, L. E. Brus, T. F. Heinz, J. Hone, and S. M. Ryu, ACS Nano **4**(5), 2695 (2010).
[26]D. Wolverson, S. Crampin, A. S. Kazemi, A. llie, and S. J. Bending, ACS Nano **8**(11), 11154 (2014).
[27]P. Hartman and W. G. Perdok, Acta Crystallogr. **8**(31), 49 (1955).